DOI: 10.1002/ejic.200700602

Synthesis and Characterization of Bis(dithiolene) Tungsten(VI), -(V), and -(IV) Complexes and Their Reactivities in Coupled Electron–Proton Transfer: A New Series of Active Site Models of Tungstoenzymes

Hideki Sugimoto,*[a] Makoto Tarumizu,[a] Hiroyuki Miyake,[a] and Hiroshi Tsukube[a]

Keywords: Bioinorganic chemistry / Enzyme models / Molybdenum / S ligands / Tungsten

New tungsten(VI), -(V), and -(IV) complexes containing 3,6-dichloro-1,2-benzenedithiolate ($bdtCl_2$), $(Et_4N)_2[W^{VI}O_2(bdtCl_2)_2]$ {$(Et_4N)_2$[**1**]}, $(Et_4N)[W^{V}O(bdtCl_2)_2]$ {(Et_4N)[**2**]}, and $(Et_4N)_2[W^{IV}O(bdtCl_2)_2]$ {$(Et_4N)_2$[**3**]} were synthesized and characterized as active site models of tungstoenzymes. $(Et_4N)_2$[**1**] was prepared in high yield by the reaction of WO_2Cl_2 with $2bdtCl_2$ at low temperature, and its crystal structure was determined. Isomerization between octahedral structures (Δ and Λ forms) of the tungsten center of $(Bu_4N)_2$[**1**] was characterized by variable-temperature ^1H NMR (VT ^1H NMR) spectral analysis, which offers the first example of six-coordinate bis(dithiolene) tungsten(VI) complexes. The isomerization of the molybdenum center of $(Bu_4N)_2[Mo^{VI}O_2(bdtCl_2)_2]$ {$(Bu_4N)_2$[**4**]} was similarly characterized. A comparison of their activation energies indicated that the tungsten center underwent slower isomerization than that of the molybdenum one. $(Et_4N)_2$[**1**] underwent an irreversible reduction at –2.1 V vs. SCE in CH_3CN by a coupled electron–proton transfer (CEPT) process to yield $(Et_4N)_2$[**3**], while $(Et_4N)_2$[**3**] underwent an irreversible oxidation by a CEPT process at –0.27 V in the presence of 2 equiv. of Et_4NOH in CH_3CN to yield $(Et_4N)_2$[**1**]. (Et_4N)[**2**] disproportionated into 0.5 equiv. of $(Et_4N)_2$[**1**] and 0.5 equiv. of $(Et_4N)_2$[**3**] when treated with 1 equiv. of Et_4NOH in CH_3CN.

Introduction

Since the characterization of tungstoenzymes by crystallographic and EXAFS studies,[1] many coordination chemists have paid much attention to intriguing coordination structures of their catalytic centers.[2] Mononuclear tungsten complexes containing two pyranopterin dithiolenes occur as the catalytic centers of the aldehyde ferredoxin oxidoreductase (AOR) family and the formate dehydrogenase (FDH) family, varying the oxidation number between +6, +5, and +4 and the coordination structure between that of a trigonal prism and a square pyramid (Scheme 1).[1,3] Therefore, synthetic tungsten(VI), -(V), and -(IV) complexes with identical dithiolenes are of special interest as active site models of these families.[2] However, such a series of tungsten complexes is still limited.[2] A number of six-coordinate bis(dithiolene) tungsten(VI) complexes have been prepared and structurally characterized.[2] The tungsten(VI) centers of the previously reported six-coordinate complexes were best described as octahedrons, rather than trigonal prisms, in the solid state, while their solution structures have rarely been reported. In contrast, a large number of $[WX(dithiolene)_2]^{2-/-}$ (X = monodentate ligand) complexes containing a square-pyramidal tungsten(IV) center have been reported.[2]

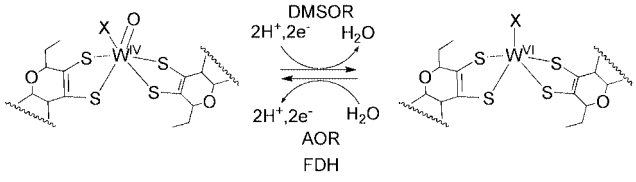

Scheme 1. Active site structures of DMSOR, AOR, and FDH families and their CEPT processes (X = O, OR, SR, SeR, etc.).

From the viewpoint of the functions of the AOR and the FDH families, a coupled electron–proton transfer (CEPT) process is essentially involved in the catalytic reactions, where the five-coordinate tungsten(IV) center changes to the six-coordinate tungsten(VI) center and a water molecule is utilized as the source of an oxygen atom, protons, and electrons.[1,3] A similar structural change of a tungsten center by the CEPT process is involved in tungsten-substituted DMSO reductase, where the six-coordinate tungsten(VI) center changes to the five-coordinate tungsten(IV) center, converting a net oxygen atom of DMSO to water.[3] The CEPT process is further involved in the catalytic reaction mediated by molybdenum containing arsenite oxidase.[1] Until now, no involvement of the bis(dithiolene) tungsten

[a] Department of Chemistry, Graduate School of Science, Osaka City University,
Sumiyoshi-ku 3-3-138, Osaka 558-8585, Japan
Fax: +81-6-6605-2522
E-Mail: sugimoto@sci.osaka-cu.ac.jp

complex in a CEPT process has been reported. We recently demonstrated that the CEPT process enabled the conversion from $(Et_4N)_2[MoO_2(bdtCl_2)_2]$ {$(Et_4N)_2$[**4**]} to $(Et_4N)_2$-$[MoO(bdtCl_2)_2]$ {$(Et_4N)_2$[**5**]} and its back reaction from $(Et_4N)_2$[**5**] to $(Et_4N)_2$[**4**].[5,6] Our crystallographic study on a series of $(X)_2[M(bdtCl_2)_3]$ (X = Et_3NH, Et_4N, Ph_4P; M = Mo, W) complexes revealed that the metal centers can adopt both trigonal-prismatic and octahedral structures depending on the size of the counter cations.[7] A similar conversion between a trigonal prism and an octahedron was not observed in other $(X)_2[M(dithiolene)_3]$ (M = Mo and W) complexes.

We herein report the synthesis and characterization of the novel $(Et_4N)_2[WO_2(bdtCl_2)_2]$ {$(Et_4N)_2$[**1**]}, $(Et_4N)[WO(bdtCl_2)_2]$ {(Et_4N)[**2**]}, and $(Et_4N)_2[WO(bdtCl_2)_2]$ {$(Et_4N)_2$-[**3**]} complexes. The structural isomerization of the tungsten center of $(Bu_4N)_2$[**1**] in [D_8]THF is characterized using the variable-temperature ^1H NMR (VT ^1H NMR) spectroscopic technique. Conversions between $(Et_4N)_2$[**1**] and $(Et_4N)_2$[**3**] by a CEPT process are described. The UV/Vis, IR, and EPR spectroscopic studies of the reaction of (Et_4N)[**2**] with Et_4NOH indicate that (Et_4N)[**2**] disproportionated into 0.5 eqiv. $(Et_4N)_2$[**1**] and 0.5 equiv. $(Et_4N)_2$[**3**] and that the disproportionation is involved in the conversion of $(Et_4N)_2$[**3**] to $(Et_4N)_2$[**1**]. Since $(Et_4N)_2$[**1**] and $(Et_4N)_2$[**3**] are isostructural complexes of $(Et_4N)_2$[**4**] and $(Et_4N)_2$[**5**], the present study is useful for understanding roles of the tungsten centers of the AOR and the FDH families (Figure 1).

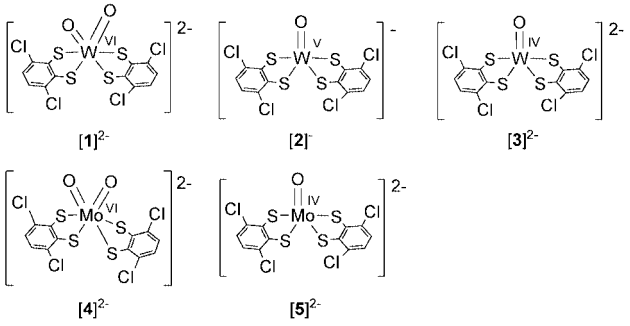

Figure 1. Structures of tungsten and molybdenum complexes.

Results and Discussion

Preparation of $W^{VI}O_2$ and $W^{IV}O/W^{V}O$ Complexes of $bdtCl_2$

Three synthetic methods have been established for bis(dithiolene) $W^{VI}O_2$ complexes. In the synthesis of $(Bu_4N)_2$-$[WO_2(mnt)_2]$, Na_2WO_4, starting compound, was treated with Na_2mnt and $NaHSO_3$ at pH 5.5 (yield 59%).[2a] Several bis(dithiolene) $W^{VI}O_2$ complexes of bdt and its derivatives were obtained in modest yields (1–15%) by several steps {$WCl_6 \rightarrow [WOCl_3(THF)_2] \rightarrow [WO(SC_6H_5)_4]^- \rightarrow [WO(SC_6H_5)_4]^{2-} \rightarrow [WO(benzendithiolates)_2]^{2-} \rightarrow [WO_2$-$(benzendithiolates)_2]^{2-}$}.[8,9] The yields of bis(dithiolene) $W^{VI}O_2$ complexes of aliphatic dithiolenes were also modest (20–30%) because the following reactions were required {$[Ni(dithiolene)_2] \rightarrow [W(CO)_2(dithiolene)_2] \rightarrow [WO(dithiolene)_2]^{2-} \rightarrow [WO_2(dithiolene)_2]^{2-}$}.[10] Here, we directly synthesized the bis(dithiolene) $W^{VI}O_2$ complex of $bdtCl_2$ from commercially available reagents. When WO_2Cl_2 was treated with 2 equiv. of H_2bdtCl_2 and 2 equiv. of Et_4NI or Bu_4NBr in the presence of 4 equiv. of Et_3N at –40 °C, a red microcrystalline powder of $(Et_4N)_2$[**1**] or $(Bu_4N)_2$[**1**] precipitated in 65% yield. (Et_4N)[**2**] and $(Et_4N)_2$[**3**] were prepared according to literature procedures by Nakamura et al. and Holm et al.[8,11]

Crystal Structure of $(Et_4N)_2[WO_2(bdtCl_2)_2]$

Figure 2 shows the crystal structure of the anionic part of $(Et_4N)_2$[**1**]. Selected bond lengths and angles are shown

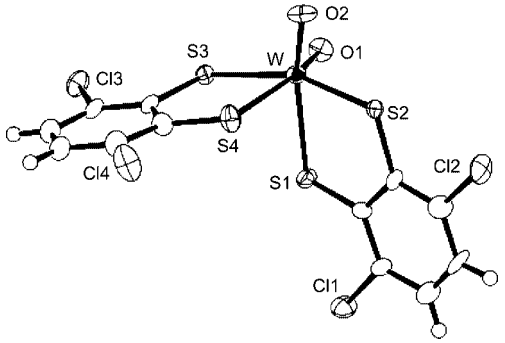

Figure 2. Crystal structure of $[1]^{2-}$ shown with 50% ellipsoids.

Table 1. Selected bond lengths [Å] and angles [°] for $(Et_4N)_2$-$[WO_2(bdtCl_2)_2]$ {$(Et_4N)_2$[**1**]} and $(Et_4N)_2[MoO_2(bdtCl_2)_2]$ {$(Et_4N)_2$-[**4**]}.

	$(Et_4N)_2$[**1**]	$(Et_4N)_2$[**4**][a]
M–O1	1.741(6)	1.726(3)
M–O2	1.749(7)	1.739(3)
M–S1	2.563(2)	2.596(1)
M–S2	2.443(2)	2.4462(9)
M–S3	2.426(2)	2.4486(9)
M–S4	2.592(2)	2.561(1)
C1–S1	1.72(1)	1.741(3)
C2–S2	1.762(9)	1.755(4)
C7–S3	1.766(8)	1.750(4)
C8–S4	1.707(9)	1.728(4)
O1–M–O2	102.6(3)	103.2(1)
M–S1–C1	108.5(3)	108.2(1)
S1–M–S2	79.71(7)	78.90(4)
S1–M–S3	85.72(7)	86.07(4)
S1–M–S4	85.55(7)	85.85(5)
S1–M–O1	88.6(2)	87.9(1)
S1–M–O2	160.3(2)	160.5(1)
S2–M–S3	159.21(7)	158.97(5)
S2–M–S4	84.64(7)	85.01(4)
S2–M–O1	111.0(3)	111.1(1)
S2–M–O2	81.2(2)	82.0(1)
S3–M–S4	79.49(7)	79.30(4)
S3–M–O1	83.2(3)	81.5(1)
S3–M–O2	111.4(2)	112.5(1)
S4–M–O1	162.0(3)	160.2(1)
S4–M–O2	88.2(2)	89.0(1)
M–S2–C2	111.1(3)	111.6(6)
M–S3–C7	111.3(3)	110.8(1)
M–S4–C8	108.0(3)	108.4(2)

[a] Ref.[5]

in Table 1. The tungsten center was coordinated by two oxo groups in a *cis* position and four sulfur atoms from the two $bdtCl_2$ ligands in a similar fashion to that observed for $(Et_4N)_2$[**4**].[5] The geometry around the metal centers of $(Et_4N)_2$[**1**] and $(Et_4N)_2$[**4**] is described as a distorted-octahedral structure on the basis of the torsion angles[4a] made by the four sulfur atoms {S2–S1–S3–S4, 101.1° for $(Et_4N)_2$[**1**] and 100.4° for $(Et_4N)_2$[**4**]}. The W=O bond lengths [1.749(7) Å and 1.741(6) Å] of $(Et_4N)_2$[**1**] are not significantly different from those of $(Et_4N)_2$[**4**]. The W–S2 and W–S3 distances [2.563(2) Å and 2.592(2) Å, respectively] of $(Et_4N)_2$[**1**] are longer than the W–S1 and W–S4 distances [2.443(2) Å and 2.426(2) Å, respectively] due to the *trans* influence of the two W=O bonds. The long W–S (2 and 3) bond lengths and the short W–S (1 and 4) bond lengths affect the S–C bond lengths of $(Et_4N)_2$[**1**]. The S1–C1 and S4–C8 bonds [1.762(9) Å and 1.766(8) Å, respectively] are longer than the S2–C2 and S3–C7 bonds [1.72(1) Å and 1.707(9) Å, respectively].

VT ^{1}H NMR Spectroscopic Study of $[MO_2(bdtCl_2)_2]^{2-}$ (M = W and Mo)

As described in the crystal structural study, the tungsten center of $[WO_2(bdtCl_2)_2]^{2-}$ ([**1**]$^{2-}$) offers two distinguishable S atoms in one $bdtCl_2$ ligand, consequently, two protons on one $bdtCl_2$ ligand, Ha and Hb, are not equivalent in the crystal structure. Unexpectedly, the ^{1}H NMR spectra of $(Bu_4N)_2$[**1**] at 25 °C in [D_6]acetone, [D_3]acetonitrile, and [D_8]THF show one singlet at δ = 6.61 ppm in the aromatic region, revealing that the Ha and Hb protons are apparently equivalent in solution.[12] This singlet broadens as the [D_8]THF solution temperature decreases from +40 °C to –60 °C. Two separate peaks are observed at –70 °C and each peak is further divided into two peaks at –90 °C (Figure 3). The singlet from $bdtCl_2$ of $(Bu_4N)_2$[**4**] similarly broadens at low temperature and is divided into two peaks at –110 °C (Figure 3). When the temperature of the [D_8]THF solutions of $(Bu_4N)_2$[**1**] and $(Bu_4N)_2$[**4**] was again increased to +40 °C their original ^{1}H NMR spectra at +40 °C were regenerated. Since these VT ^{1}H NMR spectral changes are independent of the complex concentrations, $(Bu_4N)_2$[**1**] and $(Bu_4N)_2$[**4**] exhibit structural isomerisation between the octahedral structures (50% Δ and 50% Λ forms, Scheme 2) without dissociation of the M–S bonds in solution. The trigonal-prismatic structures probably occur in the transition states where the structural isomerization of the metal center of $(Bu_4N)_2$[**1**] and $(Bu_4N)_2$[**4**] is faster than the NMR timescale at high temperatures.

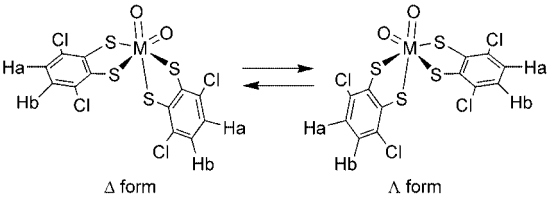

Scheme 2. Structural isomerization of anions of $(Bu_4N)_2$[**1**] and $(Bu_4N)_2$[**4**].

Δ*G* values for the isomerizations of $(Bu_4N)_2$[**1**] and $(Bu_4N)_2$[**4**] were calculated to be 43.2 and 36.4 kJ mol^{-1}, respectively, which are similar to the energy difference (37.2 kJ mol^{-1}) between the octahedron and the trigonal prism of $[Mo^{VI}(OCH_3)(OSMe_2)(S_2C_2Me_2)_2]^-$.[4a] The fact that the value of Δ*G* calculated for $(Bu_4N)_2$[**1**] is larger than that for $(Bu_4N)_2$[**4**] means that the tungsten center is kinetically more stable than the molybdenum one. This is consistent with the fact that the AOR family of tungsten enzymes belongs to the hyperthermophilic archaea.

Redox Properties of $[W^{VI}O_2(bdtCl_2)_2]^{2-}$ and $[WO(bdtCl_2)_2]^{-/2-}$

Figure 4 shows a cyclic voltammogram of $(Et_4N)_2$[**1**] in CH_3CN. $(Et_4N)_2$[**1**] undergoes one irreversible reduction at E_{pc} = –2.1 V vs. SCE, indicating that the octahedral structure of the tungsten center is unstable below –2.1 V. The coulometric measurement during the electrolysis at –2.2 V indicated that 2.3 electrons were consumed for the completion of the electrolysis. The electrolysis at –2.2 V caused the color to change from orange to pale yellow. Since the resulting pale yellow species exhibited an identical absorption spectrum and CV to those of $(Et_4N)_2$[**3**], $(Et_4N)_2$-[**1**] was suggested to change to $(Et_4N)_2$[**3**] by a two-electron-reduction coupled process accompanied by H_2O production, with contaminant protons arising from the CH_3CN solution (Scheme 3).

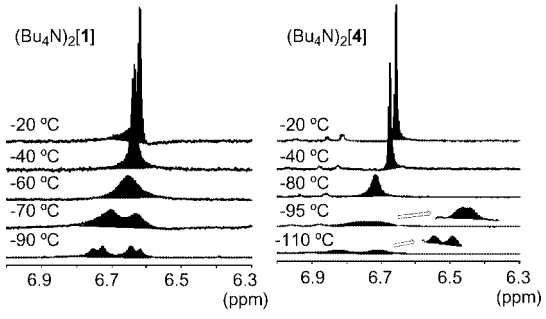

Figure 3. VT ^{1}H NMR spectra of $(Bu_4N)_2$[**1**] (4.1 mM, left) and $(Bu_4N)_2$[**4**] (4.1 mM, right) in [D_8]THF.

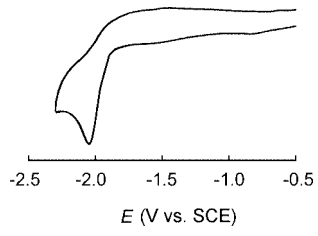

Figure 4. Cyclic voltammogram of $(Et_4N)_2$[**1**] (0.1 mM, 100 mV s^{-1}) in 0.1 M $TBAPF_6$ containing CH_3CN.

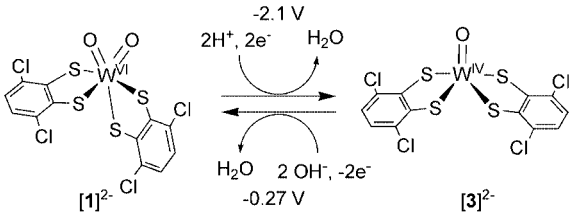

Scheme 3. Reversible structural change between $(Et_4N)_2$[**1**] and $(Et_4N)_2$[**3**] via CEPT processes.

$(Et_4N)_2$[**3**] shows one reversible oxidation wave at –0.27 V [Figure 5 (solid line)] in CH_3CN, which is assigned to the $[WO(bdtCl_2)_2]^{2-/-}$ process. The redox potential is more positive than those of $[WO(bdt)_2]^{2-/-}$ (–0.63 V) and $[WO(naphthalenedithiolate)_2]^{2-/-}$ (–0.52 V),[8,9] suggesting that the Cl atoms attached to the benzene ring decrease the S → W electron donations. Because the isostructural $Mo^{IV}O$ complex, $(Et_4N)_2$[**5**], changes to the $Mo^{VI}O_2$ complex, $(Et_4N)_2$[**4**], in the presence of 2 equiv. of OH^- under oxidative conditions,[6] the CV change of $(Et_4N)_2$[**3**] was investigated. The reversible $W^{V/IV}$ couple at –0.27 V became an irreversible wave upon addition of Et_4NOH to the CH_3CN solution of $(Et_4N)_2$[**3**], increasing the current intensity of the E_{pa} while decreasing that of the E_{pc}. The CV change depended on the added amount of Et_4NOH, and was completed when 2 equiv. of Et_4NOH and 1 equiv. of $[WO(bdtCl_2)_2]^{2-}$ was added to the solution (dashed line in Figure 5). The absorption spectrum of the orange solution obtained after electrolysis of $(Et_4N)_2$[**3**] at –0.1 V in the presence of 2 equiv. of Et_4NOH was identical to that of $(Et_4N)_2$[**1**]. The coulometric measurement taken during the electrolysis indicated that 1.9 electrons were consumed for the completion of the electrolysis. Thus, $(Et_4N)_2$[**3**] was revealed to be converted to $(Et_4N)_2$[**1**] by the CEPT process as in the case of the isostructural molybdenum complex, $(Et_4N)_2$[**5**]. Since $(Et_4N)_2$[**3**] was also changed to $(Et_4N)_2$[**1**] by the CEPT process, the tungsten center coordinated with two $bdtCl_2$ ligands was demonstrated to be convertible between the six-coordinate $W^{VI}O_2$ structure, $(Et_4N)_2$[**1**], and the five-coordinate $W^{IV}O$ structure, $(Et_4N)_2$[**3**], by CEPT processes (Scheme 3).

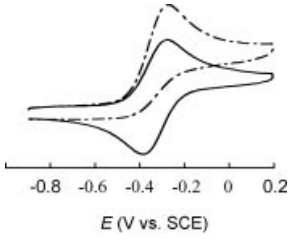

Figure 5. Cyclic voltammograms of $(Et_4N)_2$[**3**] (0.1 mM, 100 mV s^{-1}): complex only (solid line) and complex + 2 equiv. of Et_4NOH (dashed line) in 0.1 M $TBAPF_6$ containing CH_3CN.

The absorption spectrum of $(Et_4N)_2$[**3**] in CH_3CN remained the same when 2 equiv. of Et_4NOH was added, indicating that the tungsten(IV) center does not bind OH^-. Whereas (Et_4N)[**2**] reacted with Et_4NOH. When Et_4NOH was added to the CH_3CN solution of (Et_4N)[**2**] the absorption band at 600 nm decreased while the bands at 470 nm and 421 nm increased (Figure 6). The plots of absorbance at 600 nm and 421 nm against the equivalence of the added Et_4NOH per (Et_4N)[**2**] indicated that (Et_4N)[**2**] reacted with 1 equiv. of OH^- (Figure 6, inset). The anisotropic EPR signal at g_{av} = 1.96 for (Et_4N)[**2**] completely disappeared when 1 equiv. of Et_4NOH was added. In the IR spectrum of (Et_4N)[**2**] the $\nu(W^{5+}{=}O)$ stretching band at 953 cm^{-1} also disappears with the appearance of three new bands at 911, 892, and 848 cm^{-1} when 1 equiv. of Et_4NOH is added. The band at 911 cm^{-1} is identical to the $\nu(W^{4+}{=}O)$ stretching band of $(Et_4N)_2$[**3**] and the other two bands are identical to the $\nu(W^{6+}{=}O)_{sym}$ and $\nu(W^{6+}{=}O)_{asym}$ stretching bands of $(Et_4N)_2$[**1**] (Figure 7). Thus, it is concluded that the disproportionation of (Et_4N)[**2**], when treated with 1 equiv. of Et_4NOH in CH_3CN, yields 0.5 equiv. of $(Et_4N)_2$[**1**] and 0.5 equiv. of $(Et_4N)_2$[**3**] [Equation (1)], where $(Et_4N)_2[W^{V}O(OH)(bdtCl_2)_2]$ was proposed as an intermediate involved in the conversion process from $(Et_4N)_2$[**3**] to $(Et_4N)_2$[**1**].

$$2[W^{V}O(bdtCl_2)_2]^- + 2OH^- \rightarrow [W^{VI}O_2(bdtCl_2)_2]^{2-} + [W^{IV}O(bdtCl_2)_2]^{2-} + H_2O \quad (1)$$

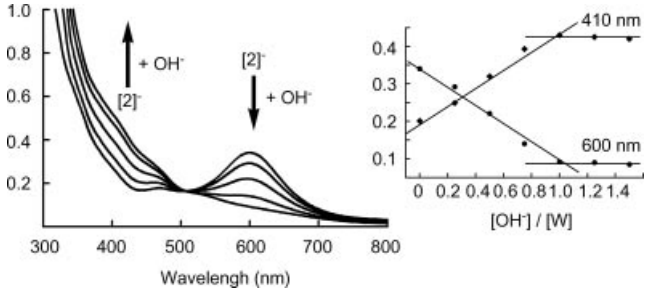

Figure 6. Absorption spectral changes of (Et_4N)[**2**] (1.7×10^{-4} M) upon addition of *n* equiv. of Et_4NOH in CH_3CN (left). Titration plots of the absorbance at 410 and 600 nm (right) against the *n* values.

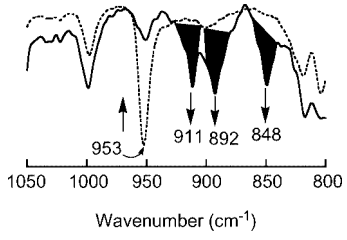

Figure 7. IR spectra of (Et_4N)[**2**] (dashed line) and an equimolar mixture (solid line) of (Et_4N)[**2**] and Et_4NOH.

Conclusion

Tungsten(VI), -(V), and -(IV) complexes with two $bdtCl_2$ ligands were synthesized and characterized as a new series of active site models of tungstoenzymes as well as tungsten-

substituted DMSO reductase. The tungsten center of $(Et_4N)_2$[**1**] adopted an octahedral structure and underwent isomerization between the Δ and Λ forms. This is the first observation involving six-coordinate bis(dithiolene) tungsten(VI) complexes. Its isomerization rate was slower than that of the isostructural molybdenum(VI) complex, [**4**]$^{2-}$. $(Et_4N)_2$[**1**] changed to $(Et_4N)_2$[**3**] by the CEPT process below –2.1 V vs. SCE, whereas $(Et_4N)_2$[**3**] was similarly converted to $(Et_4N)_2$[**1**] above –0.27 V in the presence of 2 equiv. of Et_4NOH. $(Et_4N)_2[W^VO(OH)(bdtCl_2)_2]$ was suggested to be an intermediate in the CEPT process from $(Et_4N)_2$[**3**] to $(Et_4N)_2$[**1**].

Experimental Section

General: All reagents and solvents were used as received unless otherwise noted. CH_3CN was dried with CaH_2 and then P_2O_5, and distilled under nitrogen prior to use. All manipulations were carried out under argon in Schlenk tubes. $(Bu_4N)_2[MoO_2(bdtCl_2)_2]$ {$(Bu_4N)_2$[**4**]} was synthesized by a procedure that was reported in the literature.[5,6]

$(Et_4N)_2[WO_2(bdtCl_2)_2]$ {$(Et_4N)_2$[1]}: WO_2Cl_2 (87 mg, 0.3 mmol) was added to an ethanol solution (15 mL) containing H_2bdtCl_2 (126 mg, 0.60 mmol), Et_3N (169 μL, 1.2 μmol), and Et_4NI (231 mg, 0.9 mmol) at –40 °C. After stirring for 10 h at 0 °C, the orange solution that was obtained was concentrated to 3 mL. An orange microcrystalline powder precipitated, which was collected and dried in vacuo. Yield: 174 mg (65%). $C_{28}H_{44}Cl_4N_2O_2S_4W$ (894.59): calcd. C 37.59, H 4.96, N 3.13; found C 37.64, H 4.85, N 3.07. ESI-mass: *m*/*z* = 764 [(M + $Et_4N)^-$], 634 [$(M)^-$]. UV/Vis spectrum (CH_3CN): λ (ε, $dm^3\,mol^{-1}\,cm^{-1}$) = 470 (sh, 1320), 421 (2820), 344 (sh, 13300) nm. IR (KBr): $\tilde{\nu}_{max}$ = 892 [$\nu(W{=}O)_{sym}$] and 848 [$\nu(W{=}O)_{asym}$] cm^{-1}. Raman (solid): $\tilde{\nu}_{max}$ = 893 [$\nu(W{=}O)_{sym}$] and 848 [$\nu(W{=}O)_{asym}$] cm^{-1}.

$(Bu_4N)_2[WO_2(bdtCl_2)_2]$ {$(Bu_4N)_2$[1]}: The synthesis was carried out in the same manner as that of $(Et_4N)_2$[**1**] using Bu_4NBr instead of Et_4NI. The UV/Vis and IR spectral profiles based on the anion were consistent with those of $(Et_4N)_2$[**1**].

$(Et_4N)[WO(bdtCl_2)_2]$ {(Et_4N)[2]}: The synthesis was carried out by a similar procedure to that of $(Et_4N)[WO(bdt)_2]$ reported by Holm et al.[11] A CH_3CN solution (5 mL) of 3,6-dichloro-1,2-benzenedithiol (55 mg, 0.26 mmol) and Et_3N (73 μL, 0.52 mmol) was slowly added to a CH_3CN solution (5 mL) of $(Et_4N)[WO(benzenethiol)_4]$ (100 mg, 0.13 mmol) at –40 °C. The temperature of the solution was increased to 25 °C and the resultant solution was stirred for 1 h. The deep blue solution that was obtained was reduced to a volume of 1 mL. Diffusion of ether into the solution gave a black powder, which was collected by filtration and dried in vacuo. Yield: 66 mg (68%). $C_{20}H_{24}Cl_4NOS_4W$ (748.34): calcd. C 32.10, H 3.23, N 1.87; found C 32.21, H 3.38, N 2.04. ESI-mass: *m*/*z* = 618 [$(M)^-$]. UV/Vis spectrum (CH_3CN): λ (ε, $dm^3\,mol^{-1}\,cm^{-1}$) = 600 (2050), 468 (1070) nm. IR (KBr): $\tilde{\nu}_{max}$ = 953 [$\nu(W{=}O)$] cm^{-1}.

$(Et_4N)_2[WO(bdtCl_2)_2]$ {(Et_4N)[3]}: A CH_3CN solution (2 mL) of Et_4NBH_4 (4 mg, 0.027 mmol) was added to a THF solution (10 mL) of $(Et_4N)_2$[**2**] (20 mg, 0.027 mmol). After the solution was stirred for 30 min a white yellow powder precipitated out of the solution, which was collected by filtration and dried in vacuo. Yield: 19 mg (82%). $C_{28}H_{44}Cl_4N_2OS_4W$ (878.60): calcd. C 38.28, H 5.05, N 3.19; found C 38.50, H 4.95, N 3.20. ESI-mass: *m*/*z* = 748 [M + $Et_4N^+]^-$, 618 $[M]^-$. UV/Vis spectrum (CH_3CN): λ (ε, $dm^3\,mol^{-1}\,cm^{-1}$) = 415 (1200), 330 (11100) nm. IR (KBr): $\tilde{\nu}_{max}$ = 911 [$\nu(W{=}O)$] cm^{-1}.

Other Measurements: ^1H NMR spectra were measured with a JEOL-Lambda 300. IR and Electronic spectra were recorded with a Perkin–Elmer Spectrum One and a Shimazu-U2550 spectrometer at room temperature. CV measurements and bulk electrolyses were performed with a Hokuto HZ-3000, and the working and counter electrodes were a glassy-carbon disk and a platinum wire, respectively. The complex solutions of 1.0 mM (complexes = 0.01 mmol) were deoxygenated with a stream of nitrogen gas. The reference electrode that was used was SCE. The coulometric measurements performed during the electrolyses were recorded with a Hokuto HF-201 coulomb/ampere meter.

Calculation of Activation Free Energies ($\Delta G^{\ddagger}$ Values): The values were calculated according to the equation $\Delta G/RT_c = 22.96 + \ln(T_c/\delta\nu)$, where T_c and $\delta\nu$ are the coalescence point and the frequency difference between sites in the exchange system, respectively.[13] T_c = –65 and $\delta\nu$ = 32.5 for (Bu_4N)[**1**], and T_c = –95 and $\delta\nu$ = 34.4 for (Bu_4N)[**4**] were employed.

X-ray Crystallographic Study: A single crystal of (Et_4N)[**1**] was recrystallized from acetonitrile/ether and mounted on top of a glass fiber. X-ray data of the crystal were collected with graphite-monochromated Mo-K_α radiation with a Rigaku/MSC Mercury CCD diffractometer at –130 °C. The structure was solved by direct methods (SIR-97)[14] and expanded using the program DIRDIF 99.[15] The structure was refined anisotropically by full-matrix least-squares on F^2. The non-hydrogen atoms in the structure were attached at the idealized positions on carbon atoms and not refined. The structure converted in the final stages of the refinement showed no movement in the atom positions. All calculations were performed using Single-Crystal Structure Analysis Software, Ver. 3.6.0.[16] Further crystal data and agreement factors are listed in Table 2.

Table 2. Crystallographic data for $(Et_4N)_2[WO_2(bdtCl_2)_2]$ {$(Et_4N)_2$-[**1**]}.

	$(Et_4N)_2$[**1**]
Formula	$C_{28}H_{44}Cl_4N_2O_2S_4W$
Molecular weight ($g\,mol^{-1}$)	894.57
Temperature (°C)	–130
Crystal system	orthorhombic
Space group	*Fdd*2
a (Å)	28.113(6)
b (Å)	21.888(4)
c (Å)	22.688(4)
V (Å^3)	13961(5)
Z	16
$D_{calcd.}$ ($g\,cm^{-3}$)	1.702
Unique data	18901
Observed data	7323
R	0.0460
wR	0.1200
GOF	1.001

CCDC-616400 contains the supplementary crystallographic data for this paper. These data can be obtained free of charge from The Cambridge Crystallographic Data Centre via www.ccdc.cam.ac.uk/data_request/cif.

Acknowledgments

This work was partly supported by the Japan Society for Promotion of Science, Grant No. 18750052 to H. S.

[1] a) R. Hille, *Chem. Rev.* **1996**, *96*, 2757–2816; b) M. K. Johnson, D. C. Rees, M. W. W. Adams, *Chem. Rev.* **1996**, *96*, 2817–2839; c) S. J. N. Burgmayer, *Prog. Inorg. Chem.* **2004**, *52*, 491–532.
[2] a) S. K. Das, D. Biswas, R. Maiti, S. Sarkar, *J. Am. Chem. Soc.* **1996**, *118*, 1387–1397; b) E. S. Davis, G. M. Aston, R. L. Beddoes, D. Collison, A. Dinsmore, A. Docrat, J. A. Joule, C. R. Wilson, C. D. Garner, *J. Chem. Soc. Dalton Trans.* **1998**, 3647–3656; c) J. Jiang, R. H. Holm, *Inorg. Chem.* **2004**, *43*, 1302–1310; d) J. H. Enemark, J. J. A. Cooney, J.-J. Wang, R. H. Holm, *Chem. Rev.* **2004**, *104*, 1175–1200; e) J. McMaster, J. M. Tunney, C. D. Garner, *Prog. Inorg. Chem.* **2004**, *52*, 539–583. Authors' examples: f) H. Sugimoto, M. Harihara, M. Shiro, K. Sugimoto, K. Tanaka, H. Miyake, H. Tsukube, *Inorg. Chem.* **2005**, *44*, 6386–6392; g) H. Sugimoto, T. Sakurai, H. Miyake, K. Tanaka, H. Tsukube, *Inorg. Chem.* **2005**, *44*, 6927–6929; h) H. Sugimoto, R. Tajima, T. Sakurai, H. Ohi, H. Miyake, S. Itoh, H. Tsukube, *Angew. Chem. Int. Ed.* **2006**, *45*, 3520–3522.
[3] a) M. K. Chan, S. Mukund, A. Kletzin, M. W. W. Adams, D. C. Rees, *Science* **1995**, *267*, 1463–1469; b) H. Schindelin, C. Kisker, J. Hilton, K. V. Rajagopalan, D. C. Rees, *Science* **1996**, *272*, 1615–1621; c) Y. Hu, S. Faham, R. Roy, M. W. W. Adams, D. C. Rees, *J. Mol. Biol.* **1999**, *286*, 899–914; d) J. M. Dias, M. E. Than, A. Humm, R. Huber, G. P. Bourenkov, H. D. Bartunik, S. Bursakov, J. Calvete, J. Caldeira, C. Carneiro, J. J. G. Moura, I. Moura, M. J. Romao, *Structure* **1999**, *7*, 65–79; e) H.-K. Li, C. Temple, K. V. Rajagopalan, H. Schindelin, *J. Am. Chem. Soc.* **2000**, *122*, 7673–7680; f) L. J. Stewart, S. Bailey, B. Bennett, J. M. Charnock, C. D. Garner, A. S. McAlpine, *J. Mol. Biol.* **2000**, *299*, 593–600.
[4] a) C. E. Edwin, M. B. Hall, *J. Am. Chem. Soc.* **2001**, *123*, 5820–5821; b) A. Thapper, R. J. Deeth, E. Nordlander, *Inorg. Chem.* **2002**, *41*, 6695–6702; c) M. Kaupp, *Angew. Chem. Int. Ed.* **2004**, *43*, 546–549; d) J. P. McNamara, J. A. Joule, I. H. Hiller, C. D. Garner, *Chem. Commun.* **2005**, 177–179.
[5] H. Sugimoto, M. Tarumizu, K. Tanaka, M. Miyake, H. Tsukube, *Dalton Trans.* **2005**, 3558–3564.
[6] H. Sugimoto, M. Tarumizu, H. Miyake, H. Tsukube, *Eur. J. Inorg. Chem.* **2006**, 4494–4497.
[7] H. Sugimoto, Y. Furukawa, M. Tarumizu, H. Miyake, K. Tanaka, H. Tsukube, *Eur. J. Inorg. Chem.* **2005**, 3088–3091.
[8] N. Ueyama, H. Oku, A. Nakamura, *J. Am. Chem. Soc.* **1992**, *114*, 7310–7311.
[9] H. Oku, N. Ueyama, A. Nakamura, *Bull. Chem. Soc. Jpn.* **1996**, *69*, 3139–3150.
[10] K.-M. Sung, R. H. Holm, *Inorg. Chem.* **2001**, *40*, 4518–4525.
[11] C. Lorber, J. P. Donahue, C. A. Goddard, E. Nordlander, R. H. Holm, *J. Am. Chem. Soc.* **1998**, *120*, 8102–8112.
[12] Because $(Et_4N)_2$[**1**] and $(Et_4N)_2$[**4**] did not dissolve in THF, $(Bu_4N)_2$[**1**] and $(Bu_4N)_2$[**4**] were employed.
[13] R. J. Abraham, J. Fisher, P. Loftus, *Introduction to NMR Spectroscopy*, John Wiley & Sons Ltd., England, **1988**.
[14] A. Altomare, M. Burla, M. Camalli, G. Cascarano, C. Giacovazzo, A. Guagliardi, A. Moliterni, G. Polidori, R. Spagna, *J. Appl. Crystallogr.* **1999**, *32*, 115–119.
[15] P. T. Beurskens, G. Admiraal, G. Beurskens, W. P. Bosman, R. de Gelder, R. Israel, J. M. M. Smits, **1999**. The DIRDIF-99 program system, Technical Report of the Crystallography Laboratory, University of Nijmegen, The Netherlands.
[16] *Crystal Structure Analysis Package*, Rigaku and Rigaku/MSC, **2000**–**2004**, 9009 New Trails Dr., The Woodlands, TX 77381, US.

Received: June 11, 2007
Published Online: August 28, 2007

